Synchronization of Heinrich and Dansgaard-Oeschger Events through Ice-Ocean Interactions

Logan E. Mann[1], Alexander A. Robel[1], Colin R. Meyer[2]

[1]School of Earth and Atmospheric Sciences, Georgia Institute of Technology
[2]Thayer School of Engineering, Dartmouth College

Key Points:

- The phasing of Heinrich events and DO events can be synchronized through ice-ocean interactions.
- Synchronization can explain observed phenomena despite the broad range of parameter uncertainty.
- Ice-ocean coupling regularizes the interval between DO events against noise in the climate system.

Corresponding author: Logan E. Mann, lmann7@gatech.edu

Abstract

The cause of Heinrich events and their relationship with Dansgaard-Oeschger (DO) events are not fully understood. Previous modeling studies have argued that Heinrich events result from either internal oscillations generated within ice sheets or ocean warming occurring during DO events. In this study, we present a coupled model of ice stream and ocean dynamics to evaluate the behavior of the coupled system with few degrees of freedom and minimal parameterizations. Both components of the model may oscillate independently, with stagnant versus active phases for the ice stream model and strong versus weak Atlantic Meridional Overturning Circulation (AMOC) phases for the ocean model. The ice sheet and ocean are coupled through submarine melt at the ice stream grounding line and freshwater flux into the ocean from ice sheet discharge. We show that these two oscillators have a strong tendency to synchronize, even when their coupling is weak, due to the amplification of small perturbations typical in nonlinear oscillators. In synchronized regimes with ocean-induced melt at the ice stream grounding line, Heinrich events always follow DO events by a constant time lag. We also introduce noise into the ocean system and find that the coupling not only maintains a narrow distribution of phase differences, but also regulates DO event periodicity against the effect of noise in the climate system. This synchronization persists across a broad range of parameters, indicating that it is a robust explanation for Heinrich events and their timing despite the significant uncertainty associated with past ice sheet conditions.

Plain Language Summary

Heinrich events were collapses of the North American ice sheet during the last ice age that affected the global climate significantly. Their cause is unknown. Some have theorized that the ice sheet grew over time from snow accumulation, while the earth warmed it from below. A victim of its own success, the ice may have thickened enough to insulate heat from the ground until it melted from below, lubricating its slow slide towards the ocean. This would have removed ice from land, starting the process over. However, this theory can not explain why Heinrich events occurred when they did. Later, it was theorized that Dansgaard-Oeschger (DO) events, periods of ocean warming, played a central role by triggering ice sheet collapse through melt at the ice-ocean interface. Unfortunately, we lack robust evidence that conditions were just right for the ocean to trigger these collapses repeatedly. In this paper, we describe a computational model that can reconcile the differences between these two competing theories. We propose that Heinrich and DO events can synchronize, a phenomenon where small influences between interrelated systems can align their timing. We find that this explains many mysterious aspects of the Earth's recent climate history.

1 Introduction

Heinrich events were episodic iceberg-discharge events originating from the Laurentide Ice Sheet during the last glacial period, evidenced by layers of ice-rafted debris (IRD) appearing in marine sediment records every 6-8 thousand years (Heinrich, 1988). The causes of Heinrich events and their relationship to other modes of millennial glacial climate variability remain poorly understood. Recent findings indicate Heinrich events may be causally linked to changes in the Atlantic Meridional Overturning circulation (AMOC) (Hulbe et al., 2004; Marcott et al., 2011; Alvarez-Solas et al., 2013; Shaffer et al., 2004), as abrupt freshwater pulses into the North Atlantic may have disrupted the AMOC (Ganopolski & Rahmstorf, 2001), decreased sea ice coverage, and potentially triggered other ice sheet discharges through abrupt, switch-like changes in sea ice cover (Sayag & Tziperman, 2004). Although fast ice flow and elevated ice sheet discharge are generally associated with warm climates, Heinrich events events occurred during cold stadials of Dansgaard-Oeschger (DO) events (Bond et al., 1993), which are generally thought to have occurred as a result of

AMOC weakening approximately every 1500 years (Schulz, 2002). Though Heinrich events typically occur during these cold stadials, not all DO stadials coincided with Heinrich events, indicating a complex interaction between these two seemingly related climate phenomena.

An early model of Heinrich events (MacAyeal, 1993) posited that the Hudson Strait Ice Stream, embedded within the Laurentide Ice Sheet, alternately stagnated and surged as a result of internally generated oscillations in the temperature of ice near the bed, without connection to atmospheric or oceanic forcings. In the stagnant phase, the ice stream thickened due to a frozen bed that prevented sliding. The thick ice sheet eventually insulated and trapped enough geothermal heat at the ice-bed interface to initiate the surge phase, where significant thawing of basal ice and sliding caused elevated ice discharge evidenced by IRD layers in the North Atlantic marine sediment record. Models have demonstrated the capacity of ice streams to exhibit internally generated oscillatory behavior and generate periodic surges of IRD-laden ice stream discharge across a wide range of conditions (Tulaczyk et al., 2000b; Robel et al., 2013, 2014; Bougamont et al., 2011; Sayag & Tziperman, 2009, 2011; Mantelli et al., 2016; Meyer et al., 2019). However, recent evidence shows that Heinrich events follow (rather than precede) large reductions in the AMOC during DO events (Marcott et al., 2011), casting doubt on an exclusively ice sheet driven mechnism for Heinrich events and indicating a potentially causal role for the ocean in causing Heinrich events.

The weakening of the AMOC during DO stadials shortly before Heinrich events creates a strong argument for the role of ice-ocean interactions and likely precludes an exclusively glaciological explanation (Marcott et al., 2011). Subsequently, modeling studies have sought to explain the phasing between Heinrich and DO events in one coherent framework of ice-ocean-atmosphere interactions (Marcott et al., 2011; Alvarez-Solas et al., 2013; Bassis et al., 2017). The occurrence of Heinrich events during the cold atmospheric phases of Dansgaard-Oeschger cycles precludes an exclusively atmospheric explanation, due to the thermal driving of ice sheet disintegration. Furthermore, the lack of Heinrich events during some DO events complicates an entirely ocean-driven explanation as well. Some modeling studies have proposed that Heinrich events are a result of instability induced by the collapse of a large buttressing ice-shelf during DO stadials (Shaffer et al., 2004; Hulbe et al., 2004; Marcott et al., 2011; Alvarez-Solas et al., 2013), but this explanation does not explain the lack of Heinrich events during some DO stadials as well as the lack of evidence for large ice shelf buttressing the Hudson Strait ice stream.

Our goal in this paper is to explain four of the more notable characteristics of Heinrich events, DO events, and their relationship, under a highly uncertain range of conditions and parameters, using a simple yet robust model: 1) the timing of Heinrich Events during DO stadials, 2) ice sheet collapse during periods of cold atmospheric temperatures, 3) the lack of Heinrich events during some, but not most DO events, 4) the $\sim$1500-year quasi-periodicity of DO events.

2 Model Description

Our approach in this study captures the coupled dynamics of the ice sheet-ocean system with few degrees of freedom and minimal parameterization. We couple a flowline ice stream model with a simple ocean model (Figure 1), both having the potential for internally generated oscillations. The ice stream model is a hybrid of previous ice stream models described in Robel et al. (2013) and Robel et al. (2018), capable of reproducing the grounding line dynamics simulated in more complex ice stream models (Robel et al., 2014). The ocean overturning circulation is modeled with a simple two-box model often referred to as the 'flip-flop' model of Welander (1982), which has been shown to reproduce the behavior of much more complex 3D ocean models (Cessi, 1996). In this model,

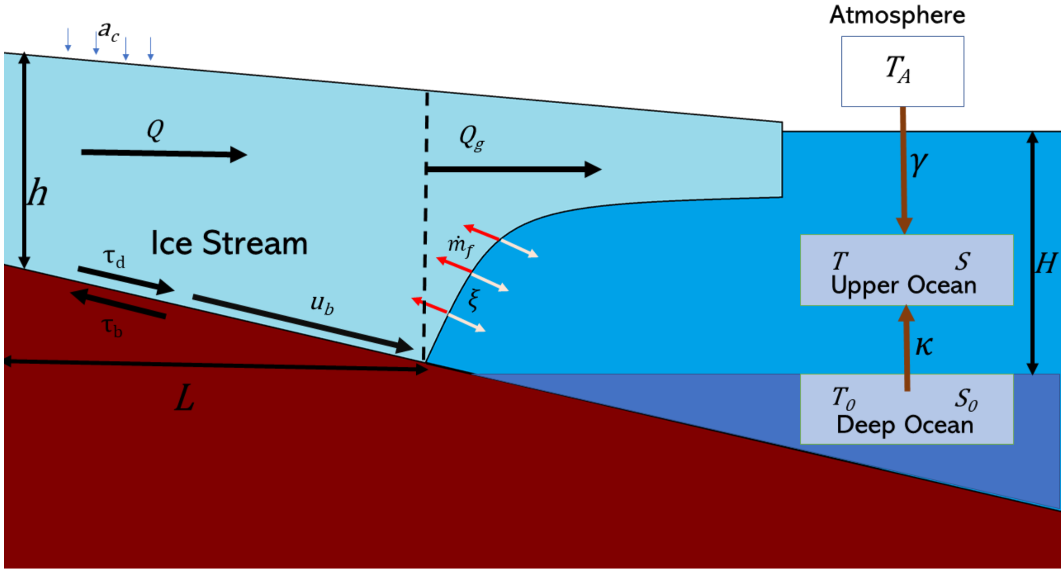

Figure 1. A diagram of the ice stream and ocean models and their interaction. Geometry is purely illustrative.

the temperature, T, and salinity, S, of the upper ocean box evolve dynamically, while the deep ocean box is assumed to be sufficiently deep that its temperature and salinity do not change. The oscillatory period of this model is varied through changes in a relaxation time constant, γ. The ice stream and ocean models are coupled through ocean-induced melt of the ice stream grounding line (with strength $\dot{m}_f$ m/yr/°C) and freshwater flux into the ocean associated with ice discharge at the grounding line (with strength ξ yr/m^2).

2.1 Ice stream model

The ice stream is represented by two boxes, one encompassing the ice stream interior and one encompassing the grounding zone. In the interior region, all spatial derivatives are averaged along the model domain, a rectangle of length L in the along-flow direction, corresponding to the grounding line position, and width W in the cross-flow direction, corresponding to width between shear margins. In initial simulations, the ice stream lies on an idealized bed with a prograde bed with a linear slope, b_x, from the ice divide, at elevation b_0, to the grounding line, at depth below sea level b_g. As described in Robel et al. (2018), mass conservation through the ice stream interior and the grounding zone requires that evolution of ice stream thickness follows

$$\frac{dh}{dt} = a_c - h\frac{Q - Q_g}{h_g L} - \frac{Q_g}{L} \tag{1}$$

where h is the spatially averaged thickness of the ice stream, a_c is the accumulation rate due to snowfall, Q is the ice flux through the interior resulting from basal sliding and deformation, Q_g is the ice flux through the grounding line, h_g is the thickness of the ice stream at the grounding line, where ice is at flotation

$$h_g = \frac{\rho_w}{\rho_i} b_g \tag{2}$$

where ρ_w and ρ_i are the densities of water and ice respectively.

The grounding line position, L, evolves dynamically as a balance of fluxes. Q transports ice from the glacier interior towards the grounding line, and Q_g transports ice from the grounding line, as in Robel et al. (2018)

$$\frac{dL}{dt} = \frac{Q - Q_g}{h_g} \tag{3}$$

Interior flux is calculated as the sum

$$Q = Q_b + Q_d \tag{4}$$

where Q_b is the ice flux from basal ice velocity which can be approximated as $Q_b = \frac{u_b h}{L}$, where u_b is the basal velocity due to till deformation, and Q_d is the flux from the deformation of ice.

For ice streams sliding over a softly Coulomb plastic bed, the grounding line flux, Q_g can be approximated as (Tsai et al., 2015)

$$Q_g = Q_0 \frac{8A_g(\rho_i g)^n}{4^n f}\left(1 - \frac{\rho_i}{\rho_w}\right)^{n-1} h_g^{n+2} \tag{5}$$

where Q_0 is a numerical coefficient constrained by boundary layer analysis, A_g is the constant creep parameter, n is the Glen's Law exponent, g is the acceleration due to gravity, and f is the Coulomb friction coefficient.

Neglecting ice deformation, Raymond (1996) calculates the centerline sliding velocity of an ice stream, upstream of the grounding line, from a balance of driving stress, τ_d, and basal shear stress, τ_b.

$$u_b = \frac{A_g W^{n+1}}{4^n(n+1)h^n}\max[\tau_d - \tau_b, 0]^n \tag{6}$$

When basal shear stress is sufficiently high, we expect most of the ice flux to be due to internal deformation within the ice column, which can be calculated as a function of driving and basal shear stresses.

$$Q_d = \frac{2A_g h^2}{n+2}\min[\tau_b, \tau_d]^n \tag{7}$$

where $\tau_d = \rho_i g \frac{h^2}{L}$ approximates the driving stress over the lumped ice stream element (Cuffey & Paterson, 2010). For soft subglacial till, τ_b is modeled as a Coulumb friction law, $\tau_b = \mu N$, where N is effective pressure and μ is a friction coefficient. Tulaczyk et al. (2000a), in laboratory measurements of till strength, showed that this can be expressed directly in terms of void ratio of the subglacial till.

$$\tau_b = \begin{cases} a'\exp(-b(e - e_c)), & \text{if } w > 0 \\ \infty, & \text{otherwise} \end{cases} \tag{8}$$

where a' is the till strength at the lower bound of void ratio, b is a constant, e is the void ratio, and e_c is the consolidation threshold of subglacial till. The void ratio is derived from a meltwater budget where w is the till water content and Z_s is the thickness the unfrozen till would reach if reduced to zero porosity. In the model, w and Z_s evolve dynamically, while e is calculated diagnostically as $e = w/Z_s$. The till water content and unfrozen till thickness evolve according to

$$\frac{dw}{dt} = m \tag{9}$$

$$\frac{dZ_s}{dt} = \begin{cases} 0, & \text{if } e > e_c \text{ or } Z_s = 0 \\ \frac{m}{e_c} & \text{if } e = e_c \text{ and } Z_0 > Z_s > 0 \end{cases} \tag{10}$$

where m is the basal melt rate, and Z_0 is the maximum sediment thickness available. Basal melt is a balance of geothermal heat flux, G, heat conduction into the ice, and heat dissipation via friction at the bed,

$$m = \frac{1}{\rho_i L_f}\left[G + \frac{k_i(T_s - T_b)}{h} + \tau_b u_b\right] \tag{11}$$

where T_s is the surface ice temperature, T_b is the basal ice temperature, k_i is the thermal conductivity of ice, L_f is the latent heat of fusion. The second term in this equation approximates the vertical heat diffusion through an ice stream (MacAyeal, 1993; Robel et al., 2014). The term $\tau_b u_b$ represents the frictional heating. It follows that negative m corresponds to the freeze-on of basal water, while positive m corresponds to melting of basal ice (Meyer et al., 2019). When $e = e_c$, both u_b and the frictional heating term are set to 0, as the till is frozen, allowing basal temperature to dynamically evolve below the melting point.

$$\begin{cases} T_b = T_m, & \text{if } w > 0 \\ \frac{dT_b}{dt} = \frac{\rho_i L_f}{C_i h_b} m, & \text{if } w = 0 \text{ and either } (T_b = T_m \text{ and } m < 0) \text{ or } (T_b < T_m) \end{cases} \tag{12}$$

where C_i is the heat capacity of ice and h_b is the thickness of the temperate basal ice layer.

2.2 Ocean model

In the ocean model adapted from Welander (1982) and Cessi (1996), there is an upper ocean box and a deep ocean box. The density of the upper ocean box is determined by an equation of state, linearized about the temperature and salinity of the deep ocean box (T_0, S_0)

$$\rho/\rho_0 = 1 + \alpha_s(S - S_0) - \alpha_T(T - T_0) \tag{13}$$

where α_s and α_T are constant expansion coefficients.

The upper ocean box is subjected to external thermohaline forcing, (e.g. continental runoff, glacial discharge, atmospheric forcings) and the deep ocean box diffusively exchanges heat and salt with the upper ocean.

$$\frac{dT}{dt} = -\gamma(T - T_A) - \kappa(T - T_0) \tag{14}$$

$$\frac{dS}{dt} = \frac{F}{H}S_0 - \kappa(S - S_0) \tag{15}$$

where γ is a time constant for relaxation of T to atmospheric temperature T_A, κ is the vertical diffusivity of heat and salt, F is the total of evaporative, precipitative, and runoff salinity fluxes into the upper ocean, and H is the depth of the upper ocean box. The time scale of vertical diffusion, κ^{-1}, depends on the vertical density gradient.

$$\kappa = \begin{cases} \kappa_1, & \text{if } \rho - \rho_0 \leq \Delta\rho \\ \kappa_2, & \text{if } \rho - \rho_0 > \Delta\rho \end{cases} \tag{16}$$

where, κ_1 is the diffusivity of heat and salt without convection, and κ_2 is the effective diffusivity associated with more rapid convective exchange between upper and deep ocean boxes. The threshold density difference, $\Delta\rho$, is a very small, negative number that activates convection, allowing rapid exchange of properties between the surface and deep boxes.

2.3 Coupling of Ice Stream and Ocean Models

The ice stream and ocean models are coupled through the modification of the grounding line flux, Qg, in equation (5).

$$Q_g = Q_0 \frac{8A_g(\rho_i g)^n}{4^n f} \left(1 - \frac{\rho_i}{\rho_w}\right)^{n-1} h_g^{n+2} - \dot{m}_f T b_g \tag{17}$$

where the added term $\dot{m}_f T b_g$ is ocean-induced melt of the grounding line. $\dot{m}_f$ is sensitivity of grounding line melt rate to temperature change (m yr^{-1} °C^{-1}) along the depth, b_g, of the ice stream at the grounding line (after Bassis et al. (2017)). In our model runs, $\dot{m}_f$ is specified on the order of 1-100 m yr^{-1} °C^{-1} of warming, consistent with observed sensitivities of contemporary marine-terminating glaciers (Rignot et al., 2016). Such melt rates, on their own, do not produce significant grounding line retreat.

To allow ice stream discharge to affect the ocean circulation, we consider the freshwater discharge associated with ice flux at the grounding line, Q_g as a negative salinity flux, in equation (15), influencing the salinity flux balance determined by F.

$$\frac{dS}{dt} = (1 - \xi Q_g)\frac{F}{H} S_0 - \kappa(S - S_0) \tag{18}$$

where ξ is the sensitivity of upper ocean salinity to changes in ice discharge (yr m^{-2}).

This coupling is implemented into the nondimensionalized equation of salinity balance in the ocean model. It follows that

$$\frac{dy}{dt} = (1 - \xi Q_g)\mu - \nu y \tag{19}$$

The freshwater flux from ice stream discharge can prolong the period between convective overturning events in the ocean model, influencing the periodicity of the DO events and lowering the amplitude of the temperature anomaly associated with DO events, reducing the effective meltrate at the grounding zone. Therefore, submarine melt and freshwater flux bidirectionally couple the ice stream and ocean models.

3 Model Results

3.1 Internal oscillations of the uncoupled ice stream and ocean models

When uncoupled from the ocean model, the ice stream is characterized by three different behaviors. In a parameter regime with warm ice surface temperature, T_s, and high geothermal heat flux, G, the ice stream basal sliding velocity, u_b, reaches an equilibrium, or 'steady streaming' state. For very low ice surface temperature and geothermal heat, the till remains frozen, preventing basal sliding. In this 'steady creep' case, the ice flux, Q, is entirely driven by deformation, resulting in a steady-state ice stream thickness and fixed grounding line position. In an intermediate parameter regime appropriate for Hudson Strait conditions during the last glacial period (see example in Figure 2a), geothermal heat and surface temperatures are sufficient to sustain internally generated oscillations between stagnant and active ice stream phases, similar to MacAyeal (1993). While the ice stream is thin, cold atmospheric temperatures conduct heat through the ice and away from the bed, maintaining a frozen till and gradual thickening of the ice stream, as a result of snowfall. Eventually, the ice stream becomes sufficiently thick to insulate the base and weaken the vertical temperature gradient, until the subglacial heat budget is positive, allowing basal ice to warm to its pressure-melting point. This meltwater production allows basal sliding to reactivate, causing a thinning of the ice stream and a temporary advance in the grounding line position, L, before rapid retreat. The behavior of this model is similar to that described in Robel et al. (2013), with the most relevant differences from this model resulting from the addition of deformation driven ice flux, which adds the possibility of 'steady creep' behavior.

The ocean component of the model simulates Dansgaard-Oeschger events as self-sustaining oscillations in upper ocean temperature, driven by periodic strengthening and weakening of the overturning circulation. When the vertical density difference exceeds a threshold density difference, the system enters a convective mode, allowing the rapid exchange of heat and salt between the shallow and deep ocean. This instability causes the system to oscillate between convecting and non-convecting states with a corresponding change in near-surface ocean temperatures (Figure 2a).

3.2 Synchronization and phase locking of the coupled ice-ocean system

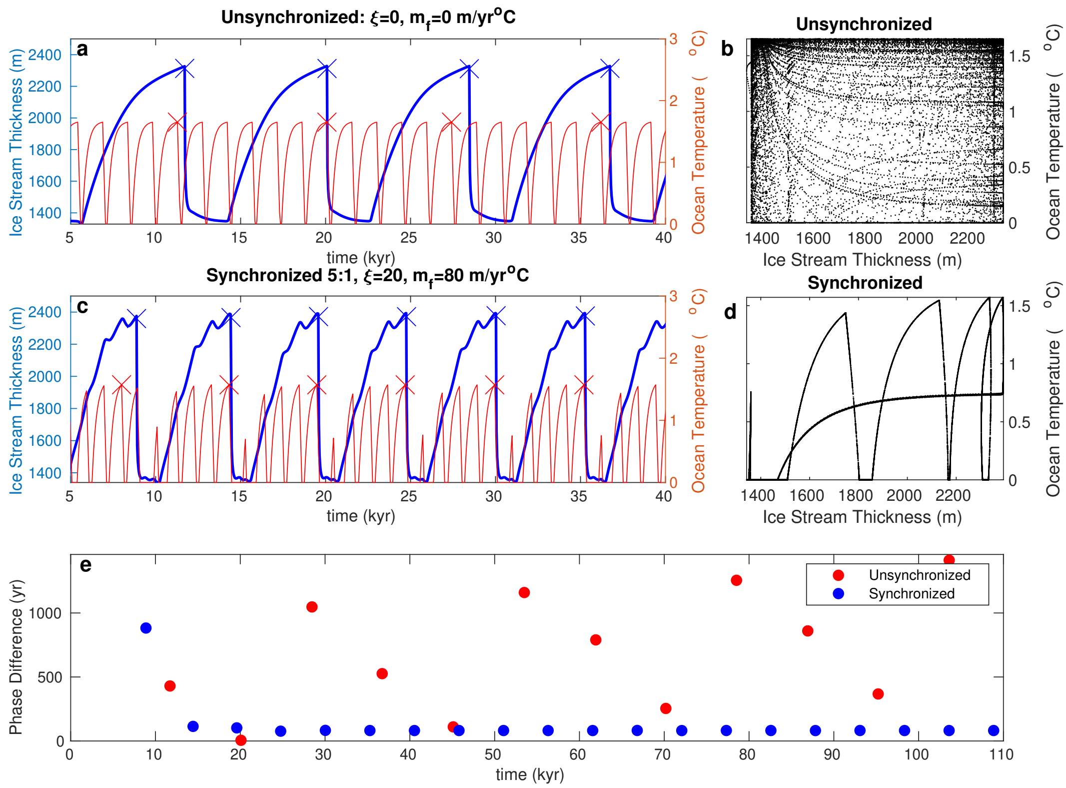

Figure 2. a) A characteristic model result when the ice stream and ocean models are not coupled. The x markings identify the onset of Heinrich events and peaks of DO event warming, through the peaks in ice stream height and ocean temperature. Here, these peaks drift apart, as the models do not influence each other. c) A characteristic model result with coupling. The phase differences of these oscillations remain near constant after a few Heinrich cycles. e) The phase differences plotted in time for each Heinrich cycle. In the unsynchronized case, phase differences have a high degree of variance. In the synchronized case, phase differences have a low variance after a small number Heinrich cycles. b,d) Ice stream height and ocean temperature plotted in 2D space. In the synchronized system, these variables mutually cycle. In the unsynchronized system, they oscillate independently.

With the ice stream and ocean models in oscillatory regimes, mutual synchronization is a possible mechanism to explain the consistent timing of Heinrich events following DO events. Synchronization occurs when autonomous oscillators have the ability to influence each other and when the strength of their coupling is sufficient to overcome their natural frequency differences, causing the oscillator phases to have a consistent difference. The canonical case of synchronization occurs in systems like weakly coupled clocks synchronizing their pendula (Huygens, 1669). Synchronization can also occur through integer frequency-ratio phase locking, meaning one oscillator may cycle many times for every one cycle of the other oscillator.

In our model, the ice stream and ocean synchronize when their coupling is strong enough to overcome the natural frequency differences of these two autonomous oscillators. Figure 2 depicts two cases; one where the models are not coupled, and the systems oscillate independently; and one where the systems are coupled and become synchronized such that there are 5 DO events for each Heinrich event and DO events are suppressed following Heinrich events. DO event warming precedes Heinrich events by hundreds of years. In the synchronized case, the time between a maximum in ocean temperature associated with a DO event and the subsequent maximum in ice discharge associated with a Heinrich event (referred to hereafter as the 'phase difference') remains constant (Figure 2c-d). In contrast, in the unsynchronized case (Figure 2a-b), the phase difference constantly drifts due to the offset between the Heinrich and DO oscillation periods. In the synchronized example, it takes a short amount of time for the system to synchronize, and the strength of the coupling reduces the variation of the phase differences to near zero (Figure 2e). This 5:1 integer frequency phase locking then remains indefinitely. With this mechanism, we reproduce the phasing of Heinrich and DO events with minimal parameterization and realistic coupling strengths.

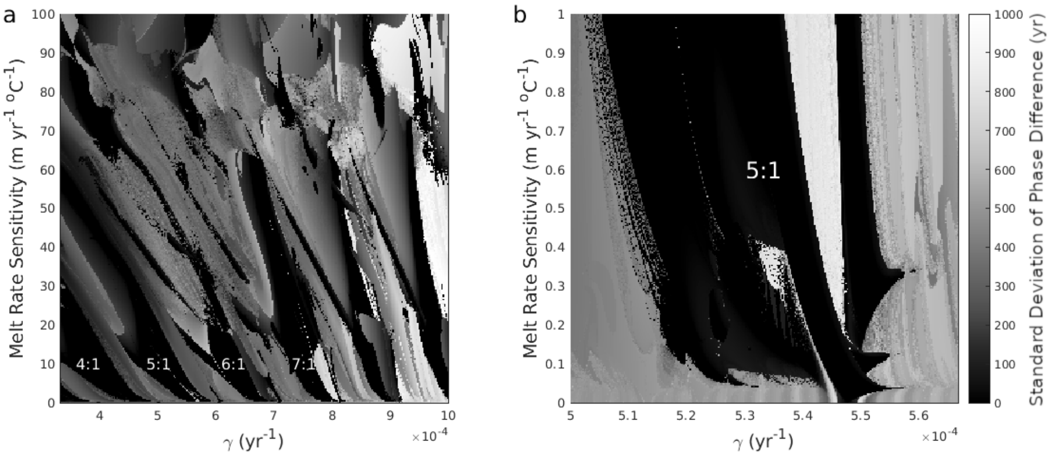

Figure 3. a) A bifurcation diagram of the one directional model, with no freshwater flux into the ocean from ice stream discharges, displaying the standard deviation of phase differences between the ice stream and ocean oscillations, over 90,000 model iterations on a 300x300 grid, covering a wide area of parameter space. γ controls the period of the ocean oscillations through the relaxation time between the atmospheric and ocean temperatures. Submarine meltrate, $\dot{m}_f$, controls the strength of of the coupling. Arnold tongues can be seen at each of the integer-frequency pairs. b) A bifurcation diagram focusing on the 5:1 Arnold tongue at meltrates lower than 1 m/yr/°C.

Synchronization will not occur in cases where the coupling is too weak and the independent oscillator frequencies are too far apart to synchronize. To characterize the robustness of synchronization behavior in this model, we sweep through parameter space of DO event period and ice-ocean coupling strength. Figure 3 shows the standard deviation of the phase difference between Heinrich events and DO events, with near-zero standard deviations indicating synchronization (i.e. the time delay from a DO event to the subsequent Heinrich event remains constant) for the case $\xi = 0$, allowing only ocean melt at the grounding line and no freshwater flux into the ocean during Heinrich events. This parameter sweep shows key features consistent with synchronized systems, primarily 'Arnold Tongues' (Arnol'd, 1961), large regions of synchronization in parameter space. In this system, an Arnold tongue exists for each of the integer-frequency phase-locked pairs (labelled in Figure 3a). The 5:1 tongue, most similar to the average period ratio between Heinrich and DO events, corresponds to cases where the model synchronizes with 5 DO events preceding every Heinrich event. We observe asymmetric Arnold tongues in our ice-ocean system, which is distinct from canonical Arnold tongues occurring in other mutually coupled systems (metronomes, pendulums clocks, etc.). Ocean melting at the grounding line can only have a destabilizing effect on the ice stream (i.e. the ocean never causes grounding line advance). Thus, ocean warming can trigger Heinrich events, but there is no ocean-mediated mechanism to prevent or prolong Heinrich events. We perform another parameter sweep focused only on a very narrow range of DO event periods and low melt rates (Figure 3b). This is intended to focus on very weakly coupled regions of the 5:1 Arnold Tongue (well below observed sensitivities of grounding line melt to ocean warming), and illustrates that, even with arbitrarily weak coupling, if the inherent frequency differences between the ice stream and ocean oscillations are small, synchronization occurs. The nonlinearities in the model amplify small perturbations of the coupling to ensure that the ice stream and ocean remain synchronized despite weak coupling.

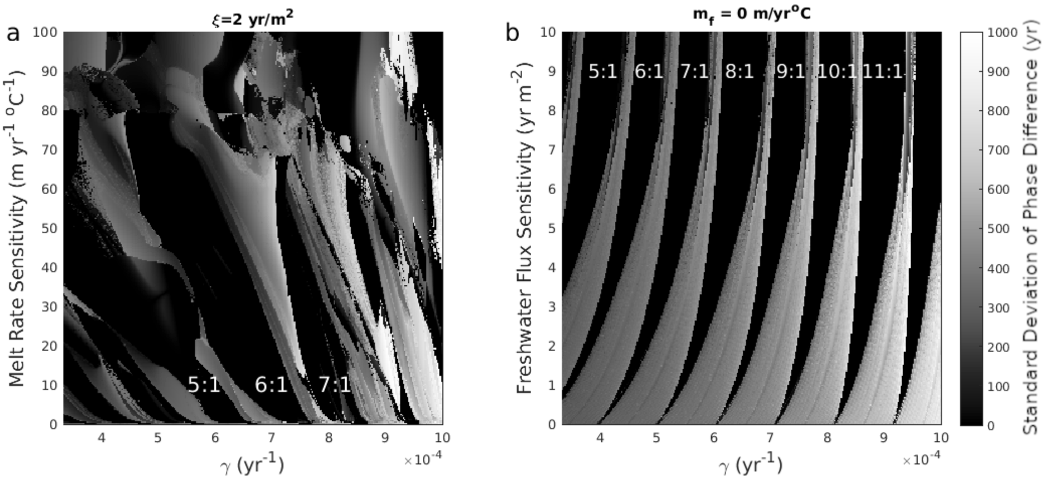

Figure 4. a) A bifurcation diagram with small freshwater fluxes enabled during ice stream discharge, covering a wide area of parameter space with respect to γ, which controls DO event period, and submarine melt rate, $\dot{m}_f$. This greatly increases the extent of Arnold Tongues and synchronized regions. b) A bifurcation diagram without any submarine melt of the ice stream, allowing only coupling through iceberg discharge, with respect to γ (relaxation time) and freshwater flux parameter, ξ.

Next, we consider the influence of coupling from the ice stream to the ocean, as a result of freshwater fluxes from ice stream discharge. As seen in Figure 2c, when this freshwater flux is significant, it can suppress the amplitude of DO events immediately following Heinrich events. Figure 4a plots a parameter sweep with bi-directional coupling, including a modest sensitivity of upper ocean salinity to ice stream discharge (ξ=2 m^2/yr). Even when this coupling is weak, the ice to ocean coupling greatly increases the prevalence of synchronization in parameter space. Figure 4b depicts the parameter space of the coupled system when only coupling from the ice stream to the ocean is active ($\dot{m}_f$ $= 0$ m/yr/°C). In this case, the period between Heinrich Events remains constant, as only the amplitude and period of the ocean oscillation can be affected by its ice stream oscillator counterpart. The simplified nature of the ocean model when compared to the ice stream model lends itself to a simpler structure of Arnold Tongues in parameter space (more similar to the canonical case of the coupled circle map (Arnol'd, 1961)). In this case, the Arnold Tongues are asymmetric with regard to relaxation time, γ (which controls DO event period). This differs from the canonical case of Arnold Tongues of a simple oscillatory system, in which tongues are represented on a domain of period and coupling strength. In this case, however, the freshwater flux from ice discharge delays the evolution of the ocean system, decreasing the period of DO events with increased coupling. However, when the period of DO events is recalculated, after the effects of coupling increase the period on model runs, the Arnold Tongues are fully vertical on a DO event period-coupling strength parameter space (see supplement Figure S2).

3.3 Stochastic forcing of the coupled ice-ocean system

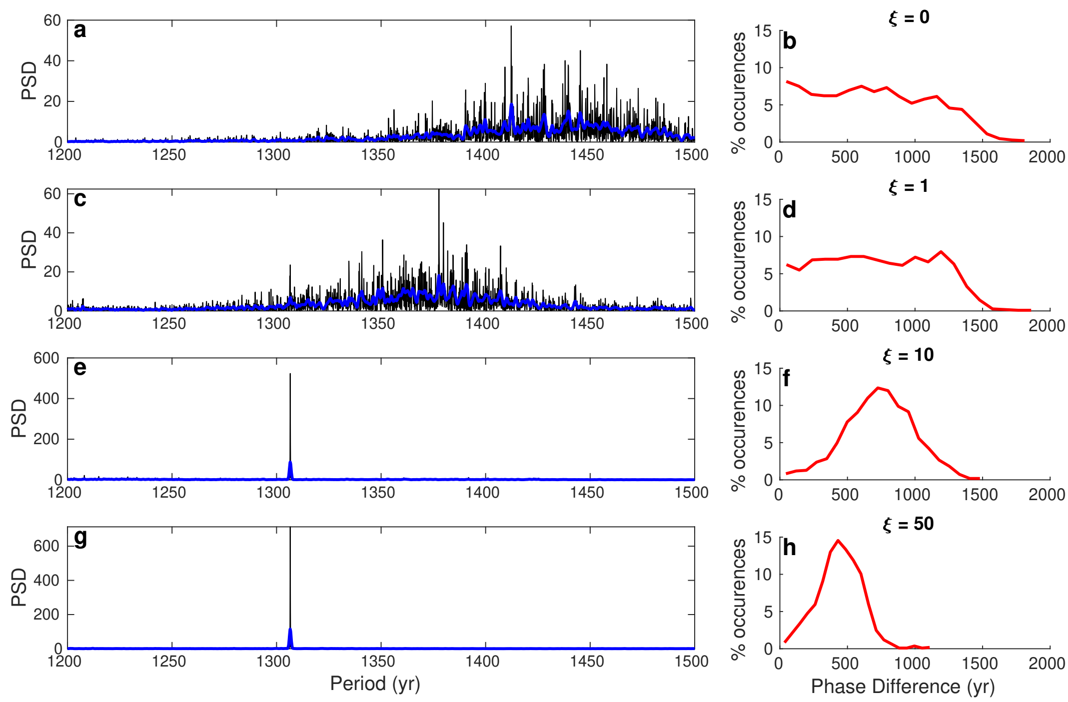

Figure 5. a,c,e,g) Power Spectral Density of ocean temperature, with respect to the period of ocean oscillations. This shows narrowing of the delta function associated with increased coupling b,d,f,h) Phase difference distribution for the stochastic model shows convergence of phase difference with increased coupling.

In reality, ice sheets and the ocean are subject to noise from the atmosphere and other more rapidly fluctuating earth system processes. Incorporating noise into our model could potentially disrupt synchronization of Heinrich and DO events, as the system may not be able to maintain consistent phase differences between ice stream and ocean oscillations under the influence of random noise. To test the influence of noise on synchronization, we add white noise to the ocean model, in a similar process to Cessi (1996) (see supplement). Figure 5a shows that even with the spectral broadening effect of noise the power spectrum for ocean temperature narrows towards a delta function around a single period as coupling sensitivity from ice discharge into the ocean (ξ) increases. Figure 5b,d,f,h shows that increased coupling also narrows the distribution of phase differences. Thus, coupling between ice sheets and the ocean not only regulates DO event periodicity in the presence of intrinsic climate noise, but also regulates the degree of synchronization, measured by consistency of phase differences between Heinrich events and DO events. This result shows that coupling between ice sheets and the ocean may be responsible not only for the synchronization of these oscillations, but also for the remarkable regularity of the ~1500 year DO event interval in the presence of climatic noise (Schulz, 2002).

3.4 Heinrich Events Resulting from GIA-Modulated Ocean Forcing

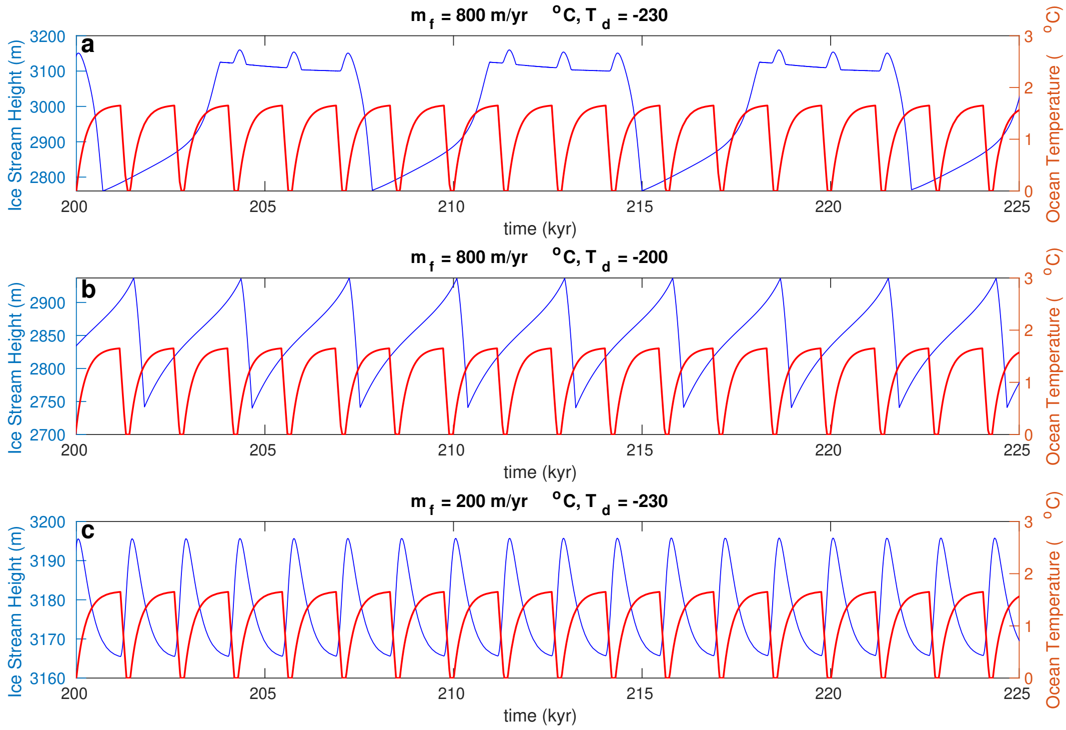

Figure 6. a) Ice stream height and near-surface ocean temperature as the bed evolves dynamically due to GIA. During the first 3-4 DO events, the ice stream is protected by an elevated sill, eventually advancing to depress the sill and on the next DO event. Small peaks in ice stream height can be observed in between Heinrich events, as the ice stream advances past the sill, before retreating back to the sill during DO events. b) The same model with the thermocline depth 30 meters higher. The sill does not adjusts high enough to limit Heinrich events to a 5:1 cycle. Large scale retreat instead occurs during every other DO event. c) The same model with a low melt rate. The grounding line never retreats sufficiently to be protected from DO event associated temperature increases.

Bassis et al. (2017) (hereafter B17) modeled Heinrich events forced by prescribed variations in ocean temperature modulated by glacial isostatic adjustment of a submarine sill. In the B17 model, Heinrich events were driven by ocean forced terminus melt and iceberg calving, rather than by the internal oscillatory dynamics of basal sliding, as in our model. DO events were prescribed as sinusoidal temperature pulses according to the timing of DO events in the marine sediment record. Isostatic adjustment of the bed was modeled with an elastic lithosphere relaxing aesthenosphere (ELRA) model (Bueller et al., 1985; Lingle & Clark, 1985). When the ice stream terminus is at its most advanced position, forward of the sill, it is grounded at a depth beneath the thermocline, and in contact with the warmer subsurface ocean. When DO events occur, the terminus rapidly retreats in response to ocean-driven terminus melt, until reaching a new equilibrium position farther upstream and beginning its slow advance. The retreat and thinning of the ice stream allows the sill to rise through GIA, bringing it above the depth of the thermocline, preventing the warmer subsurface water from accessing the terminus during subsequent DO events.

By incorporating ELRA isostatic adjustment of the along-flow bed topography including a gaussian proglacial sill and a strong melt rate sensitivity, $\dot{m}_f$, our model can reproduce the B17 mechanism for Heinrich events (Figure 6a). The ice stream component of the model is set to a thermal regime that produces non-oscillating, deformation driven ice flow. The ocean component is set to a regime that produces near-surface ocean temperature oscillations with a $\sim$1400 event period. Freshwater forcing of the ocean by iceberg discharge is eliminated.

In this version of our model, oscillations of the grounding line position occur, not because of the internal dynamics of the ice stream, but rather due to an external ocean forcing. This reproduces the conclusion of Bassis et al. (2017), that the ice stream will retreat rapidly due to forcing from warm ocean water, followed by a slow advance as the sill cuts off contact to the warm water resulting from subsequent DO events. In order for this mechanism to reproduce the phasing of Heinrich events with DO events and the periodicity of Heinrich events, it requires: (i) a high melt rate sensitivity ($\dot{m}_f$), (ii) a carefully tuned sill geometry relative to the thermocline depth, and (iii) rates of ice deformation tuned such that the terminus advances at a rate where it does not prematurely depress the sill before 5 DO cycles are complete. In Figure 6b, the thermocline depth is set slightly higher (well within the range of uncertainty or paleotopography of the Hudson Strait), such that the sill never reaches an elevation sufficient to prevent grounding line retreat. In Figure 6c, the melt-rate sensitivity is closer to realistic values, measured at modern glacier termini (Rignot et al., 2016). The ice stream never retreats behind the sill, and it instead oscillates in front of the sill during each DO event. Ultimately, the model mechanism only reproduces the observations of B17 under a very narrow range of parameters, some of which are not consistent with observed values.

4 Discussion

In our coupled model of the interaction between an ice stream and the ocean, the occurrence of synchronization, across wide swaths of parameter space, offers a potential unification of the two types of Heinrich event theories: ice-sheet only driven mechanisms and ocean-driven changes in the ice sheet. In our theory, Heinrich events are driven by the ice sheet, DO events are driven by the ocean, and the timing of the two distinct phenomena are brought into phase by ice-ocean interactions. This synchronization mechanism explains four puzzling characteristics of observations: 1) the timing of Heinrich events during DO stadials 2) ice sheet collapse during periods of cold atmospheric temperatures 3) the lack of Heinrich events following some DO events 4) the $\sim$1500-year quasi-periodicity of DO events.

This model also has key advantages over other physical explanations of Heinrich events, primarily in its ability to describe observed phenomena with fewer degrees of freedom and without fine tuning of parameters. For example, incorporating GIA into our model to simulate Heinrich events caused by ocean forcing and modulated by isostatic adjustment, we can meet all four criteria outlined above by carefully tuning model parameters. However, models of Heinrich events which are tuned to match observations may not continue to match observations under minor variations in parameters within the broad range of parameter uncertainty under paleoclimatic conditions. Synchronization provides a mechanism that can reproduce many of the most puzzling characteristics of observations over a wider range of possible parameter regimes. For example, in B17 and other models with large ocean-mediated ice stream retreats, sensitivity to melt must be high. In contrast, synchronization can explain the consistent phasing of Heinrich and DO events, even with very small meltrates. This persistence of synchronization under very weak coupling is a well known feature of a broad class of coupled nonlinear oscillators found in nature (Winfree, 2001). Thus it is perhaps unsurprising that two highly nonlinear systems with the tendency to generate internal oscillatory behavior will synchronize when coupled even weakly. At more realistic meltrates, and with bi-directional coupling, synchronized regions cover much of the parameter space, indicating that synchronization of Heinrich and DO events is not just possible, but probable.

Our synchronized system is also resilient to noise that we would expect to arise in the chaotic climate system. Coupling not only phase-locks Heinrich and DO events, but also regularizes oscillation period against noise in the ocean system. In cases with noise, coupling can still result in phase differences between Heinrich and DO events that, while not constant as in the deterministic model, are narrowly distributed, as in observations (Schulz, 2002).

5 Conclusion

In our model, we reconcile two disparate theories for Heinrich events and their relationship with DO events that resolves problems in prior theories. We provide explanations for several puzzling characteristics of the marine sediment record, in a way that remains robust over a wide range of parameters and does not require prescribed forcing. The robustness of these findings, even considering noise in the Earth system, indicates that synchronization is a strong potential explanation for Heinrich events and their relationship to DO events.

Synchronization is a relevant phenomenon in this system and many other geophysical phenomena with oscillatory components. Under the right conditions, synchronization can greatly amplify the effects of even very weak interactions, common in nonlinear systems. Investigation of interacting oscillatory modes within the Earth system requires the consideration of these effects to better understand their inter-related dynamics. With the increasing practicality of fully coupled dynamic ice sheet and climate models, operating on paleoclimatic timescales, the role of synchronization should be further investigated, both in this system and in others.

Acknowledgments

Thanks to Jean Lynch-Stieglitz and Charles Gertler for discussions during completion of this work and comments on the manuscript. Logan Mann and Alex Robel were supported by startup funds from the Georgia Institute of Technology and utilized computing resources provided by the Partnership for an Advanced Computing Environment (PACE) at the Georgia Institute of Technology, Atlanta. All model code and plotting scripts are available as public repositories from: `https://github.com/loganemann/IceStreamOcean_Coupled`

References

Alvarez-Solas, J., Robinson, A., Montoya, M., & Ritz, C. (2013). Iceberg discharges of the last glacial period driven by oceanic circulation changes. *Proceedings of the National Academy of Sciences of the United States of America*, *110*, 16350-16354.

Arnol'd, V. I. (1961). Small denominators. 1. mapping the circle onto itself. *Bulletin* *of the Russian Academy of Sciences*, *25*, 21-86.

Bassis, J. N., Petersen, S. V., & Cathles, L. M. (2017). Heinrich events riggered by ocean foring and modulated by isostatic adjustment. *Nature*, *542*, 332–334.

Bond, G., Wallace, B., Johnsen, S., McManus, J., Labeyrie, L., Jouzel, J., & Bonani, G. (1993). Correlations between climate records from north atlantic sediments and greenland ice. *Nature*, *365*, 143-147.

Bougamont, M., Price, S., Christoffersen, P., & Payne, A. (2011). Dynamic patterns of ice stream flow in a 3-d higher-order ice sheet model with plastic bed and simplified hydrology. *Journal of Geophysical Research*, *116*.

Bueller, E., Lingle, C. S., & Brown, J. (1985). Fast computation of a viscoelastic deformable earth model for ice-sheet simulations. *Annals of Glaciology*, *46*, 97-105.

Cessi, P. (1996). Convective adjustment and thermohaline excitability. *Journal of Physical Oceanography*, *26*, 481–491.

Cuffey, K., & Paterson, W. S. B. (2010). *The physics of glaciers* (4th ed.). Elsevier Scientific Publishing Company.

Ganopolski, A., & Rahmstorf, S. (2001). Rapid changes of glacial climate simulated in a coupled climate model. *Nature*, *409*, 153-158.

Heinrich, H. (1988). Origin and consequences of cyclic ice rafting in the northeast atlantic ocean during the past 130,000 years. *Quaternary Research*, *29*, 142-152.

Hulbe, C. L., MacAyeal, D. R., Denton, G. H., Kleman, J., & Lowell, T. V. (2004). Catastrophic ice shelf breakup as the source of heinrich event icebergs. *Paleoceanography*, *19*.

Huygens, C. (1669). Instructions concering the use of pendulum-watches for finding the longitude at sea. , 937-976.

Lingle, C. S., & Clark, J. A. (1985). A numerical model of interactions between a marine ice sheet and the solid earth: Application to a west antarctic ice stream. *Journal of Geophysical Research*, *90*, 1100-1114.

MacAyeal, D. R. (1993). Binge/purge oscillations of the laurentide ice sheet as a cause of the north atlantic's heinrich events. *Paleoceanography and Paleoclimatology*, *8*, 775-784.

Mantelli, E., Bertagni, M. B., & Ridolfi, L. (2016). Stochastic ice stream dynamics. *Proceedings of the National Academy of Sciences*, *113*(32), E4594–E4600.

Marcott, S. A., Clark, P. U., Padman, L., Klinkhammer, G. P., Springer, S. R., Liu, Z., … Schmittner, A. (2011). Ice-shelf collapse from subsurface warming as a trigger for heinrich events. *Proceedings of the National Academy of Sciences of the United States of America*, *108*, 13415-13419.

Meyer, C. R., Robel, A. A., & Rempel, A. W. (2019). Frozen fringe explains sediment freeze-on during heinrich events. *Earth and Planetary Science Letters*, *524*, 115725.

Raymond, C. (1996). Shear margins in glaciers and ice sheets. *Journal of Glaciology*, *42*(140), 90–102.

Rignot, E., Xu, Y., Menemenlis, D., Mouginot, J., Scheuchl, B., Li, X., … de Fleurian, B. (2016). Modeling of ocean-induced ice melt rates of five west greenland glaciers over the past two decades. *Geophysical Research Letters*, *43*, 6374-6382.

Robel, A. A., Degiuli, E., Schoof, C., & Tziperman, E. (2013). Dynamics of ice stream temporal variability: Modes, scales, and hysteresis. *Journal of Geophysical Research: Earth Surface*, *118*(2), 925–936.

Robel, A. A., Roe, G. H., & Haseloff, M. (2018). Response of marine-terminating glaciers to forcing: Time scales, sensitivities, instabilities, and stochastic dynamics. *Journal of Geophysical Research: Earth Surface*, *123*(9), 2205–2227.

Robel, A. A., Schoof, C., & Tziperman, E. (2014). Rapid grounding line migration induced by internal ice stream variability. *Journal of Geophysical Research:*

Earth Surface, *119*(11), 2430-2447.

Sayag, R., & Tziperman, E. (2004). A "triple sea-ice state" mechanism for the abrupt warming and synchronous ice sheet collapses during heinrich events. *Paleoceanography*, *19*.

Sayag, R., & Tziperman, E. (2009). Spatiotemporal dynamics of ice streams due to a triple-valued sliding law. *Journal of Fluid Mechanics*, *640*.

Sayag, R., & Tziperman, E. (2011). Interaction and variability of ice streams under a triple-valued sliding law and non-newtonian rheology. *Journal of Geophysical Research*, *116*.

Schulz, M. (2002). On the 1470-year pacing of dansgaard-oeschger warm events. *Paleoceanography*, *17*.

Shaffer, G., Olsen, S. M., & Bjerrum, C. J. (2004). Ocean subsurface warming as a mechanism for coupling dansgaard-oeschger climate cycles and ice-rafting events. *Geophysical Research Letters*, *31*.

Tsai, V. C., Stewart, A. L., & Thompson, A. F. (2015). Marine ice-sheet profiles and stability under coulomb basal conditions. *Journal of Glaciology*, *61*(226), 205–215.

Tulaczyk, S., Kamb, W. B., & Engelhardt, H. F. (2000a). Basal mechanics of ice stream b, west antarctica: 1. till mechanics. *Journal of Geophysical Research: Solid Earth*, *105*, 463–481.

Tulaczyk, S., Kamb, W. B., & Engelhardt, H. F. (2000b). Basal mechanics of ice stream b, west antarctica 2. undrained plastic bed model. *Journal of Geophysical Research: Solid Earth*, *105*, 483–494.

Welander, P. (1982). A simple heat-salt oscillator. *Dynamics of Atmospheres and Oceans*, *6*, 233-242.

Winfree, A. T. (2001). *The geometry of biological time* (2nd ed.). Springer-Verlag New York.

Supporting Information for "Synchronization of Heinrich and Dansgaard-Oeschger Events through Ice-Ocean Interactions"

Logan E. Mann[1,2], Alexander A. Robel[1], Colin R. Meyer[2]

[1]School of Earth and Atmospheric Sciences, Georgia Institute of Technology

[2]Thayer School of Engineering, Dartmouth College

Contents of this file

1. Text S1 to S4

2. Figures S1 to S4

Introduction

This supporting information provides greater detail in text on some of the methods and results in the main text of "Synchronization of Heinrich and Dansgaard-Oeschger Events through Ice-Ocean Interactions", as well as supporting figures that describe these methods and results. This document describes: 1) The nondimensionalization of the ocean model, which elaborates on the implementation and parameter selection of the ocean model from the main text, 2) The model implementation of stochastic noise, which details the numerical methods used and the code implementation, 3) The model implementation of ELRA glacial isostatic adjustment, which describes the bed topography and the implementation of ELRA GIA in the ocean forced version of the model, and 4) The Numerical methods for simulations.

Text S1. Nondimensionalization of the ocean model

Cessi (1996) shows that it is possible to nondimensionalize the ocean model of Welander (1982) and constrain parameters for oscillatory behavior in the model. This will aid in the determination of appropriate parameter regimes and in the implementation of coupling. Variables are nondimensionalized as

$$x = \frac{T - T_0}{T_A - T_0} \tag{S1}$$

$$y = \frac{\alpha_S(S - S_0)}{\alpha_T(T_A - T_0)} \tag{S2}$$

$$t' = t\gamma \tag{S3}$$

where x is the nondimensional temperature balance, y is the nondimensional salinity balance, and t' is a nondimensional time variable. Equations 14-15 in the main text are nondimensionalized as

$$\frac{dx}{dt} = 1 - x - \nu x \tag{S4}$$

$$\frac{dy}{dt} = \mu - \nu y \tag{S5}$$

where $\nu = \kappa/\gamma$ is the ratio of the relaxation and diffusion time constants and μ measures the ratio of surface salinity flux to surface temperature flux.

$$\mu = \frac{F\alpha_s S_0}{H\gamma\alpha_T(T_A - T_0)} \tag{S6}$$

ν is taken to be a function of the nondimensional density gradient, $y - x$

$$\nu = \begin{cases} \nu_1, & \text{if } y - x \leq \epsilon \\ \nu_2, & \text{if } y - x > \epsilon \end{cases} \tag{S7}$$

$\nu_1 = \kappa_1/\gamma$ is assumed to be $<< 1$, because diffusion time, κ_1^{-1} is much longer than relaxation time $\gamma_1^{-1}\nu_2 = \kappa_2/\gamma$ is an order of magnitude greater than ν_1. ϵ represents the threshold vertical density gradient beyond which convection occurs, $\epsilon = \Delta\rho_0/[\alpha_T(T_A - T_0)]$. ϵ is a very small negative number.

The advantage of this nondimensionalization is that the behavior is governed by one parameter, μ. The system will oscillate if $\mu_2 > \mu > \mu_1$, where

$$\mu_1 = \frac{\nu_1}{1+\nu_1} + \epsilon\nu_1 \tag{S8}$$

$$\mu_2 = \frac{\nu_2}{1+\nu_2} + \epsilon\nu_2 \tag{S9}$$

In this study, μ is set close to μ_2, $\mu = \mu_2 - \nu_2\delta$. As long as $\delta > 0$ and $\delta << 1$, the model remains in an oscillatory regime (Figure S1).

Text S2. Model implementation of stochastic noise

As in Cessi (1996), the ratio surface salinity flux to surface temperature flux, μ, is the sum of $\bar{\mu}$, which is equivalent to μ in the deterministic model, and Gaussian noise, $\mu'(t)$.

$$\mu = \bar{\mu} + \mu'(t) \tag{S10}$$

with the forward Euler implementation of stochastic noise being

$$\langle \mu'^2 \rangle = \sigma_s^2/\Delta t \tag{S11}$$

where $\langle\rangle$ indicate an ensemble average.

In our implementation, the randn function in MATLAB is used to add gaussian pseudorandom noise scaled to the square root of timestep Δt and standard deviation of noise σ_s. It follows that

$$\mu'(t) = \mathrm{randn} \cdot \sigma_s/\sqrt{\Delta t} \tag{S12}$$

A characteristic result for the stochastic model can be seen in Figure S3.

Text S3. Model implementation of ELRA glacial isostatic adjustment

A one-dimensional bed is initialized along the x-axis, through the addition of a gaussian-shaped sill to a linear, prograde slope (Figure S4):

$$b(x) = b_0 + b_x x + \frac{H_S}{\sigma_S\sqrt{2\pi}}\exp\left[-\frac{1}{2}\left(\frac{x-\mu_S}{\sigma_S}\right)^2\right] \tag{S13}$$

where b_0 is the ice divide height, b_x is the slope of the prograde bed, H_S is a unitless parameter that scales the height of the sill, σ_S determines the sill width, and μ_S determines the sill position.

The model implements an Elastic Lithospere Relaxing Aesthenosphere model (Lingle & Clark, 1985), to consider glacial isostatic adjustment under a single ice stream:

$$\rho_r g w + D\nabla^4 w = \sigma_{zz} \tag{S14}$$

$$\frac{\partial u}{\partial t} = -\frac{u-w}{\tau} \tag{S15}$$

where ρ_r represents the density of the aesthenosphere, g is the gravitational constant, D represents the flexural rigidity of the lithosphere, ∇^4 is the biharmonic operator, and σ_{zz} represents the ice load stress per unit area, which is a function of ice stream height, $\sigma_{zz} = -\rho_i g h$. u represents the vertical displacement of the bed, which decays to equillibrium plate displacement w on a time span determined by relaxation time, τ.

As the model here is one-dimensional with respect to x, Equation S14 is rearranged to

$$\rho_r g w + D\frac{\partial^4 w}{\partial x^4} = \sigma_{zz} \tag{S16}$$

This is discretized with the boundary conditions

$$\frac{\partial w}{\partial x}(x = -x_{\max}) = 0 \tag{S17}$$

$$\frac{\partial w}{\partial x}(x = x_{\max}) = 0 \tag{S18}$$

and solved numerically on each timestep for $w(x)$ using a fourth order finite difference method at n_x finite grid points. This solution can then be used to on the right hand side of equation S15. Each grid point of $\partial u/\partial t$ is treated as its own ODE (du/dt_1, du/dt_2, ..., du/dt_{n_x}) and solved alongside the other prognostic equations. To evaluate the system far from the boundary conditions, far field points are added to the bed geometry at the initial condition such that $B(x < 0) = B_0$ and slope decreases to zero at $\frac{3}{4}x_{\max}$.

Text S4. Numerical methods for simulations

Ordinary differential equations (ODEs) are solved in MATLAB with the ode113 function, a variable-step, variable-order (VSVO) Adams-Bashforth-Moulton PEVE solver. Absolute and Relative error tolerances are set to 10^{-9}. In the stochastic model, ODEs are solved with Forward Euler with a timestep of 1 yr. In the implementation of ELRA GIA, equation S15 is solved with a fourth order finite difference method, and each grid point of equation S14 is treated as its own ODE, solved alongside the other prognostic equations using ode113.

References

Cessi, P. (1996). Convective adjustment and thermohaline excitability. *Journal of Physical Oceanography*, *26*, 481–491.

Lingle, C. S., & Clark, J. A. (1985). A numerical model of interactions between a marine ice sheet and the solid earth: Application to a west antarctic ice stream. *Journal of Geophysical Research*, *90*, 1100-1114.

Welander, P. (1982). A simple heat-salt oscillator. *Dynamics of Atmospheres and Oceans*, *6*, 233-242.

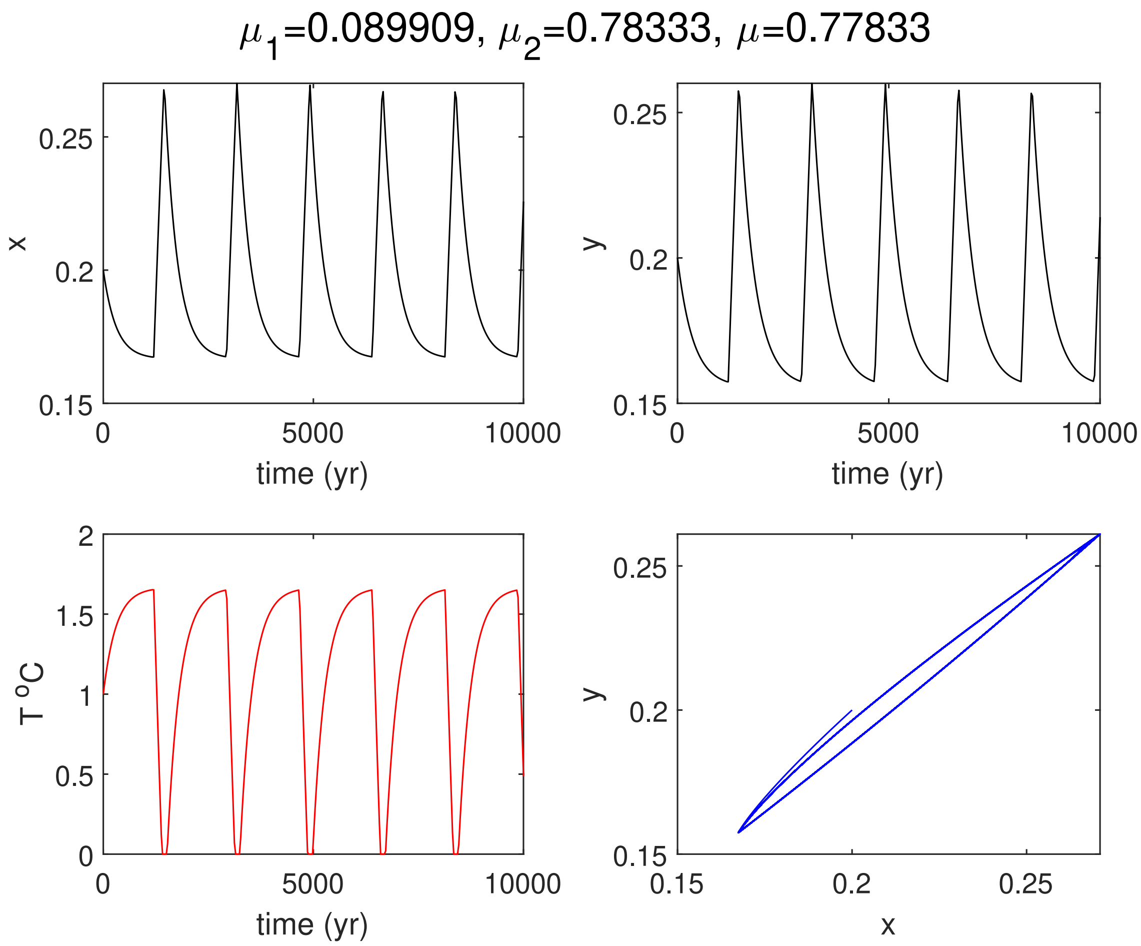

Figure S1. Self sustained thermohaline oscillations

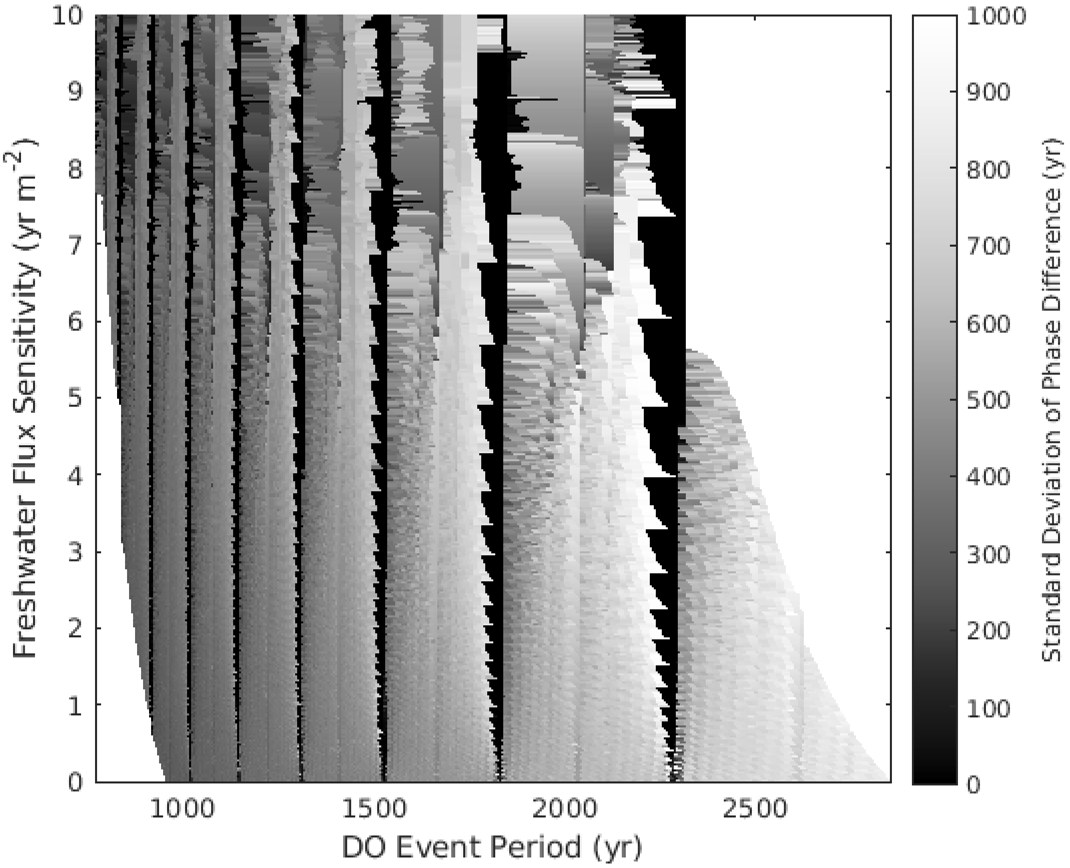

Figure S2. The results of a parameter sweep with only ice stream to ocean coupling, recalculated to the domain of DO event period and freshwater flux sensitivity (ξ yr m^{-2}). The domain is non rectangular, because the sweep is performed on the domain of relaxation time and coupling strength, and increased coupling strength alters the DO event period. This shows that Arnold Tongues are vertical on this domain. White spaces on either side are outside the domain of this sweep.

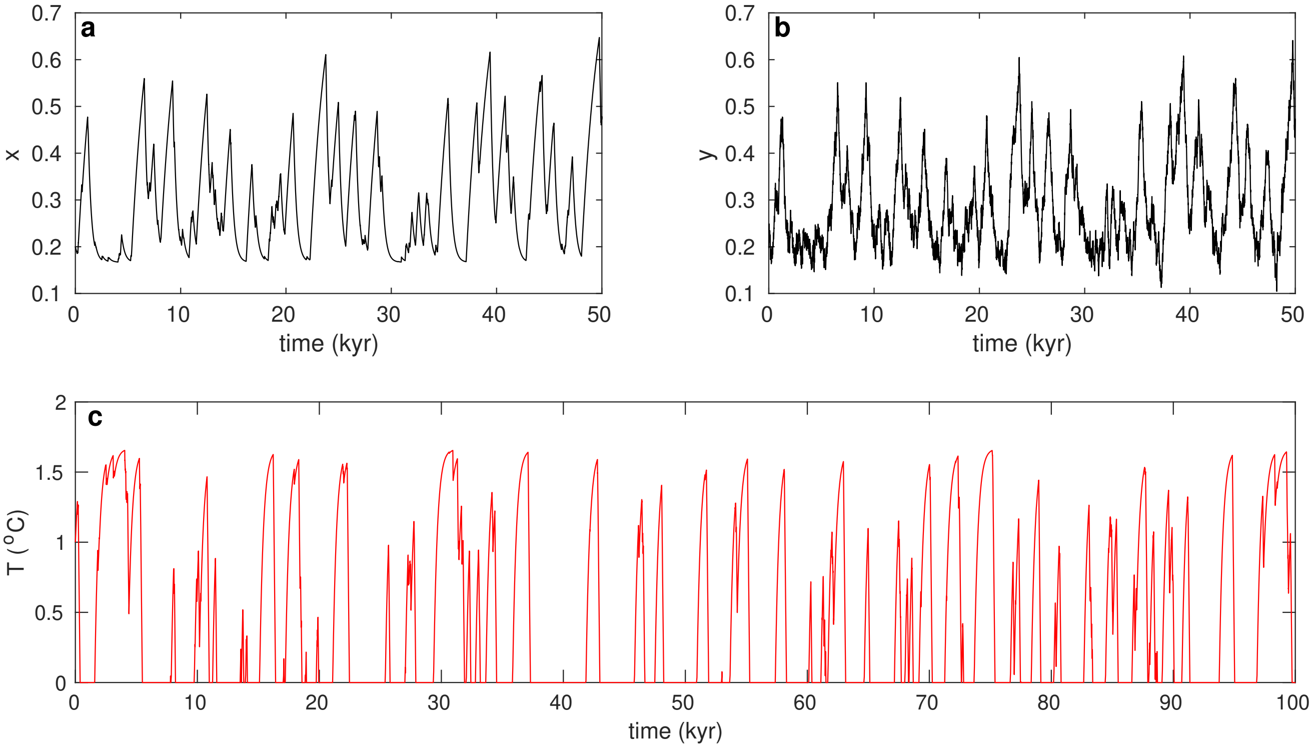

Figure S3. The stochastic model of near-surface ocean temperature with white noise with a standard deviation of $\sigma_s = 10^{-3}$ yr$^{(1/2)}$ and no coupling between ice stream and ocean systems, showing a) the nondimensional temperature variable evolving with white noise, b) the nondimensional salinity variable evolving with white noise, and c) near surface ocean temperature calculated from nondimensional parameters.

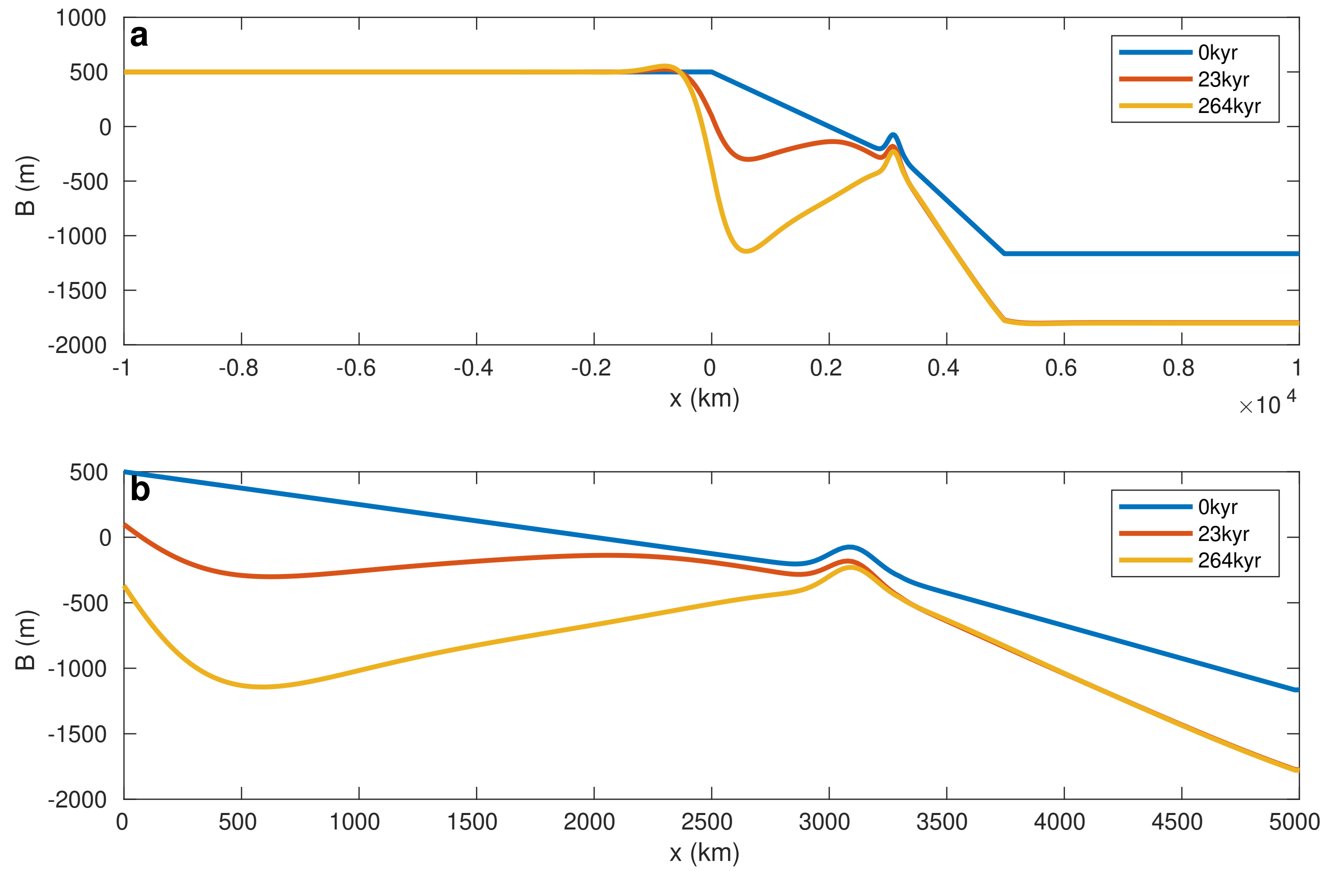

Figure S4. a) The Bed Geometry along the entire domain. Grid points below $x = 0$ km are initialized as B_0=500 m. Grid points between 0 and 5000 km are initialized with a linear prograde slope with a gaussian shaped sill near the typical grounding line position. The slope is initialized as 0 beyond the 5000 km grid point. b) The region of the bed topography initialized with a prograde slope. The weight of the ice stream eventually depresses this prograde slope into a retrograde slope, ending with the sill.